Model predictive flow control

- Invited paper -

R. King[*], K. Aleksic[*], G. Gelbert[*], N. Losse[*], R. Muminovic[*]

A. Brunn[†], W. Nitsche[†], M. R. Bothien[‡], J. P. Moeck[‡], C. O. Paschereit[‡], B. R. Noack[§]

Berlin Institute of Technology, Germany

U. Rist[¶] and M. Zengl[¶]

University of Stuttgart, Germany

In the last two decades model predictive control (MPC) has been shown to be one of the most powerful and versatile control methods in process engineering. With the availability of constantly increasing computing power and the advent of highly efficient optimization methods MPC is within reach for the use in very fast flow control applications as well. This contribution gives an introduction into MPC and reviews some examples, both in simulation studies and in experimental tests. Although a major advantage of MPC, namely the inclusion of constraints is exploited in only one of these first applications, the superiority over other control methods becomes evident. The applications range from the control of the flow around a circular cylinder, the damping of Tollmien-Schlichting waves, the suppression of thermoacoustic instabilities in a burner to the drag reduction of an Ahmed body. Models used in these MPC-studies comprise continuous and discrete-time, linear and non-linear formulations, thereby showing the versatility of the method.

Nomenclature

$\mathbf{A}, \mathbf{B}, \mathbf{C}$	state-space matrices		J	cost functional
A	amplitude		k	time index
a_i	Fourier coefficient or coefficient of time-series models		$\mathbf{Q}, \mathbf{R}$	weights
			t	time
b_i	coefficient of time-series models		$\underline{u}$	control input vector
c_p	normalized pressure		$\mathbf{U}$	velocity field
$e(t)$	error		$\underline{x}, x$	state vector, streamwise coordinate
f, g	plane pressure waves		$\underline{y}, y$	input vector, wall normal direction
G_{ls}, R_{ds}, R_{us}	transfer functions		Φ	phase of flow
H	horizon		τ	time-delay

I. Introduction

Much has been said already about the benefits of active flow control in comparison or in addition to passive means[16, 24]. To cope with uncertainties, coming either from external disturbances or from an incomplete knowledge of the flow, closed-loop flow control is a must in a real-world application. Open-loop concepts will fail or will yield at most sub-optimal results in such cases of uncertainty. For the synthesis of closed-loop

---

[*]Chair for Measurement and Control.
[†]Chair for Aerodynamics.
[‡]Chair for Experimental fluid dynamics.
[§]Chair for Theoretical fluid dynamics.
[¶]Institute of Aerodynamics and Gasdynamics.

flow controllers a variety of methods is available starting from model-free approaches to procedures which directly use a model of the system to be controlled inside the control law.

Model-free approaches as extremum- and slope-seeking control[4] perform an online gradient-based search to minimize or maximize a certain cost functional[7,45]. The determination of the gradient is done by means of a sinusoidal pertubation of the plant input. As the gradient can only be extracted when the pertubation is slower than the slowest time constant of the process, these methods are very slow. They range in the order of 10 to 100 characteristic time units of the flow system. However, extremum and slope seeking controllers are very easy to apply, and, if tuned correctly, very robust. We have successfully used these gradient-based methods in a variety of flow control configurations such as applications in high-lift, drag-reduction of different bluff-bodies, pressure recovery in diffusors, damping of thermoacoustic instabilities in a burner, mixing, and noise reduction in turbomachinery. A review of some of these applications can be found in King et al.[25]. A detailed study concerning a high-lift configuration with a swept constant chord wing is given in Becker et al.[8]. Methods to substantially accelerate extremum seeking controllers by means of an estimation of the gradient with a Kalman filter can be found in Henning et al.[21].

Another class of control synthesis methods is based on a linear black-box description of the flow. In the first place, the dynamic relation between plant inputs and outputs is described by so-called transfer functions in the Laplace- or z-domain. As flow systems are inherently nonlinear, this input-output point of view will only be valid in the vicinity of the operating conditions used to derive the model. Therefore, a family of black-box models has to be identified for different operating points and, then, has to be used in a robust controller synthesis. Popular methods comprise H_∞- or QFT-design which yield controllers applicable for a larger region of operation. Experimental flow control tests for the spanwise non-constant control of the recirculation length behind a backward facing step or the drag reduction of a 3D bluff body can be found in Henning et al.[23] and Henning et al.[22], respectively. The velocity of these methods is in the region of 1 to 10 characteristic time units of the flow system. From a control point of view this is still slow. However, this is not due to the control methods applied, but often a result of the sensor technique used to measure an appropriate on-line surrogate value indicating the state of the flow. The outcome of robust and reliable sensors very often have to be averaged, thereby reducing the bandwidth of the closed-loop system.

The fastest and/or most efficient closed-loop system response can be obtained from physically motivated controllers. These are based upon or motivated by reduced-order models such as Galerkin[33,34,41,42] or vortex models. In Pastoor et al.[36] a vortex model is used to motivate a one-sided actuation of a 2D bluff body yielding the same drag reduction as a two-sided version, but with an energy saving of more than 40%. In Gerhard et al.[18] a Galerkin model is employed to synthesize a nonlinear controller based on physical insight of the system. The obtained least-order Galerkin model describes the vortex shedding behind the circular cylinder with just three dynamical states. The controller produces a robust closed-loop performance when applied to a direct numerical simulation of the Navier-Stokes equation. In King et al.[26] different nonlinear controllers are compared for this system. Glauser et al.[19] build up a Galerkin system to derive a control law for a lift control application. Siegel et al.[42] dampen the von Kármán vortex street behind a cylinder in an experiment with a similar approach. Depending on the flow measurements available to close the loop, these methods give rise to a closed-loop bandwidth in the order of the open-loop bandwidth of the flow system.

In all of the above mentioned approaches the manipulated variable is calculated based upon the actual process output, and, more or less directly, on a process model. Neglecting the very slow extremum seeking approaches, the controllers are set up in a way to obtain a certain closed-loop dynamics without aiming at an optimal result nor respecting system constraints which may show up at the actual time instant or in the future. When a constrained optimization-based control scheme is formulated, instead, even better results can be obtained. This is shown in numerous academic and especially large scale industrial applications in process industry[20,38,39]. The basic idea of model predictive control (MPC) is a repeated optimization over a future control input trajectory. As such an optimization can be easily formulated with or without constraints, for linear or nonlinear, for time-continuous or discrete-time models, for single-input single-output (SISO) or multiple-input multiple output (MIMO) systems, MPC presents an extremely versatile method. However, as soon as constraints are involved and/or the model is nonlinear, the optimization has to be solved numerically. As a consequence of the numerical burden involved in solving the optimization problem, MPC was mainly restricted to slow processes such as found in chemical or biochemical industries. For experimental flow control applications only one burner study[17] is known up to now which will be recapitulated below. However, new efficient optimization algorithms open the route for MPC for a wider class of flow control applications as well. In a recent study, a constrained MPC was applied in an engine control problem with a sampling rate

American Institute of Aeronautics and Astronautics

of 200 Hz[15]. According to the authors, this frequency can even be increased (personal communication).

In this paper, a short introduction into MPC is given, complemented by a review of a couple of different MPC flow control applications. This selection comprises studies with linear and nonlinear, with continuous and discrete-time models, with simulation studies and experimental tests. The paper is organized as follows: The basic idea of MPC is recapitulated in section II. Applications to various configurations are given in section III.

II. Model predictive control

MPC is best explained by means of figure 1. The basic idea of MPC is to calculate future control moves such that some performance criterion is optimized. In doing so, system constraints referring to states $\underline{x}$, outputs $\underline{y}$ and manipulated variables $\underline{u}$ are respected. For this purpose, the future control input $\underline{u}_f(t)$ is parameterized by, for example, piece-wise constant trajectories over a discrete-time horizon H_c. Usually, the
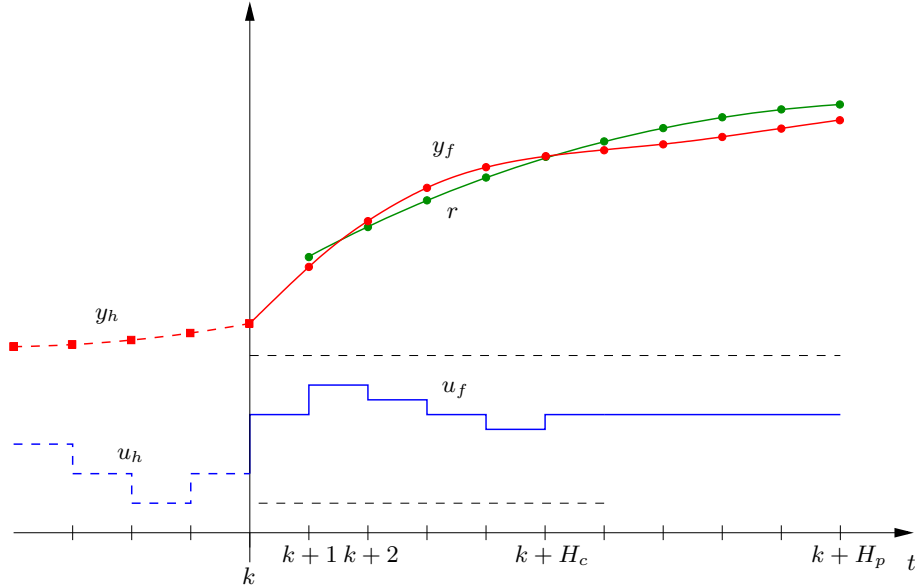

Figure 1. Basic scheme of MPC for a SISO system. In contrast to the standard fluid dynamics nomenclature, control engineering naming conventions are used here. The manipulated variable is denoted by u and the system output by y. Indices f and h refer to the future and the past, i.e. history, respectively. The reference signal r is specified starting from $k+1$, because the actual system output $y(k)$ cannot be changed by the actual or future inputs.

sampling period h for the piece-wise constant control input is fixed. It coincides with the sampling period of the model if a discrete-time model of the process is used. In the study of the von Kármán street it coincides with half the period of the flow. A variable sampling period, however, is possible as well, see e.g.[44].

Let us assume that the actual discretized time instant is given by $t = k$. Hence, $t < k$ represents the past and $t > k$ the future. The actual control input for $t = k$, i.e. $\underline{u}(k) = \underline{u}_f(k)$, and future control inputs $\underline{u}_f(k+1)$, $\underline{u}_f(k+2)$, ... are now determined such that the system output $\underline{y}_f(k+i)$ is driven back to a reference trajectory $\underline{r}(k+i)$ for $H_1 \leq i \leq H_p$ in an optimal fashion. If a system with a pure time-delay d is considered, the output $\underline{y}$ will not be influenced by the actual input $\underline{u}(k)$ before $t = k + d$. In such cases, H_1 should be equal or larger than d. Even without time-delays, a $H_1 > 1$ might be beneficial for the overall performance.

Due to the piece-wise constant control input a finite parametric optimization problem results with optimization or design variables $\underline{u}_f(k), \underline{u}_f(k+1), \ldots$. The prediction horizon H_p is usually chosen (much) larger than the control horizon H_c in which control moves are allowed. A larger prediction horizon in comparison to the control horizon is beneficial for closed-loop stability. Otherwise, a terminal penalty has to be included[39]. A possible criterion or quality function may read

$$J = \sum_{i=H_1}^{H_p} ||\underline{r}(k+i) - \underline{y}_f(k+i)||_{\mathbf{Q}} + \sum_{i=0}^{H_c} ||\underline{u}_f(k+i)||_{\mathbf{R}} \stackrel{!}{=} \min \quad , \tag{1}$$

American Institute of Aeronautics and Astronautics

in which $\mathbf{Q}$ and $\mathbf{R}$ are symmetric weighting matrices used in the norms $||\cdot||$, i.e. $||\underline{z}||_{\mathbf{S}} = \underline{z}^T \mathbf{S} \underline{z}$. Both weights may depend on the time index $k+i$ as well. With the weights a different importance of manipulated values $\underline{u}_f(k+i)$ and future errors between reference $\underline{r}(k+i)$ and system output $\underline{y}_f(k+i)$ is accounted for. If changes in the control input $\Delta \underline{u}_f(k+i) = \underline{u}_f(k+i) - \underline{u}_f(k+i-1)$ are critical to avoid too large actuator amplitudes from one sampling instant to the next, these changes can be included in eq. (1) readily. Likewise, if the future control input for $t > k + H_c$ is not zero, its cost can be included as well. When constraints have to be considered, these can be dealt with via Lagrange operators or via penalty functions to name just two possibilities.

So far it was assumed that the optimal control input calculated after processing the measurement obtained at $t = k$ could be immediately applied at the same time instant. If the numerical burden is high, however, the measurements taken at $t = k$ are used to calculate the next control moves starting from $t = k + 1$. In such a case, the second summation in eq. (1) would start at $i = 1$.

In MPC, just the first control move $\underline{u}_f(k)$ of the calculated optimal input trajectory is applied to the plant. To react almost immediately when the next measurement $\underline{y}$ for $t = k + 1$ ist obtained, preparatory calculations can be done in the period from k to $k + 1$. Then, the optimization starts from the beginning at the next sampling instant. By this, the influence of unknown disturbances and model errors is accounted for as these uncertainties show up in the next value of the measured output variable $\underline{y}(k+1)$. This repeated solution of an optimization problem has led to an alternative name of MPC, namely receding horizon optimal control.

In the general case, when the process model is nonlinear, a numerical solution of the optimization problem has to be done. This leads to a nonlinear model predictive controller (NMPC). A similar approach has to be taken for linear models in case of equality or inequality constraints which have to be met. This numerical solution, however, is responsible for the large numerical burden involved in solving (N)MPC problems. The beauty of the (N)MPC-method rests in its unifying framework. Irrespective of the kind of model, linear or nonlinear, continuous or discrete-time, SISO or MIMO, and irrespective or the optimization problem to be solved, unconstrained or constrained, the same principle can be used to derive a control signal.

To show the most simplest version of a MPC-scheme which leads to an explicit control law, a couple of assumptions will be made in the following. It is assumed that 1) the process model is given as a linear, discrete-time state-space model, 2) the plant output $\underline{y}(k)$ at time k will not directly depend on the control input $\underline{u}(k)$, i. e. there is no direct feed through, 3) the time for evaluating the control law obtained can be neglected, and 4) no constraints are considered.

II.A.   MPC formulation for linear unconstrained problems in state-space

Every linear system can be described by a state-space model of the form

$$\underline{x}(k+1) = \mathbf{A}\underline{x}(k) + \mathbf{B}\underline{u}(k) \tag{2}$$
$$\underline{y}(k) = \mathbf{C}\underline{x}(k) \tag{3}$$

in which $\underline{x}, \underline{u}$ and $\underline{y}$ represent the internal state of the process, the control input and the process output, respectively. Column vectors are denoted by small, underlined symbols. Matrices, such as the dynamic matrix $\mathbf{A}$, the input and the output matrices $\mathbf{B}$ and $\mathbf{C}$, respectively, are given in bold capital letters. A time-dependence of these matrices can be included. Dimensions are $\underline{x} \in \mathbb{R}^n$, $\underline{u} \in \mathbb{R}^p$, $\underline{y} \in \mathbb{R}^q$, $\mathbf{A} \in \mathbb{R}^{n \times n}$, $\mathbf{B} \in \mathbb{R}^{n \times p}$, $\mathbf{C} \in \mathbb{R}^{q \times n}$.

Starting from time k, the future development of the process can be predicted exploiting eq. (2). If a state prediction made at $t = k$ for $t = k + j$ is denoted by $\underline{x}(k+j|k)$, it follows

$$
\begin{aligned}
\underline{x}(k+1|k) &= \mathbf{A}\underline{x}(k) + \mathbf{B}\underline{u}(k) \\
\underline{x}(k+2|k) &= \mathbf{A}\underline{x}(k+1|k) + \mathbf{B}\underline{u}(k+1) \\
&= \mathbf{A}^2\underline{x}(k) + \mathbf{A}\mathbf{B}\underline{u}(k) + \mathbf{B}\underline{u}(k+1) \\
&\vdots \\
\underline{x}(k+H_p|k) &= \mathbf{A}^{H_p}\underline{x}(k) + \sum_{i=0}^{H_p-1} \mathbf{A}^i \mathbf{B}\underline{u}(k+H_p-1-i) \quad .
\end{aligned} \tag{4}
$$

Hence, the future or predicted output for $k + j$ reads

$$\underline{y}_f(k+j) = \underline{y}(k+j|k) = \mathbf{CA}^j \underline{x}(k) + \sum_{i=0}^{j-1} \mathbf{CA}^i \mathbf{B} \underline{u}_f(k+j-1-i) \tag{5}$$

in which $\underline{u}$ was replaced by $\underline{u}_f$ as future values of the control input are addressed. All future outputs will now be concatenated in $\underline{y}_p = (\underline{y}^T(k+1|k)\ \underline{y}^T(k+2|k)\ldots\underline{y}^T(k+H_p|k))^T$, where ^{T} denotes the transpose of a vector. Accordingly, $\underline{u}_p = (\underline{u}_f^T(k)\ \underline{u}_f^T(k+1)\ \ldots\ \underline{u}_f^T(k+H_c)\ldots\underline{u}_f^T(k+H_p))^T$ with $\underline{u}_f(k+j) = \underline{u}_f(k+H_c)$ for $j = H_c+1, H_c+2,\ldots,H_p$ to account for a constant manipulated variable for the last section of the prediction horizon H_p.

All future outputs inside the prediction horizon can now be written as

$$\underline{y}_p = \mathbf{A}_p \underline{x}(k) + \mathbf{B}_p \tilde{\underline{u}}_p \tag{6}$$

with

$$\mathbf{A}_p = \begin{pmatrix} \mathbf{CA} \\ \mathbf{CA}^2 \\ \vdots \\ \mathbf{CA}^{H_c} \\ \vdots \\ \mathbf{CA}^{H_p} \end{pmatrix}, \quad \mathbf{B}_p = \begin{pmatrix} \mathbf{CB} & \mathcal{O} & \ldots & \mathcal{O} \\ \mathbf{CAB} & \mathbf{CB} & \ldots & \mathcal{O} \\ \vdots & \vdots & \ddots & \vdots \\ \mathbf{CA}^{H_c}\mathbf{B} & \mathbf{CA}^{H_c-1}\mathbf{B} & \ldots & \mathbf{CB} \\ \mathbf{CA}^{H_c+1}\mathbf{B} & \mathbf{CA}^{H_c}\mathbf{B} & \ldots & \mathbf{CB}+\mathbf{CAB} \\ \vdots & \vdots & \ddots & \vdots \\ \mathbf{CA}^{H_p-1}\mathbf{B} & \mathbf{CA}^{H_p-2}\mathbf{B} & \ldots & \sum_{i=0}^{H_p-H_c-1}\mathbf{CA}^i\mathbf{B} \end{pmatrix}, \quad \tilde{\underline{u}}_p = \begin{pmatrix} \underline{u}_f(k) \\ \underline{u}_f(k+1) \\ \vdots \\ \underline{u}_f(k+H_c) \end{pmatrix} \tag{7}$$

In the new variables $\underline{y}_p$, $\tilde{\underline{u}}_p$, the cost functional, eq. (1), reads with $\underline{r}_p = (\underline{r}^T(k+1)\ \underline{r}^T(k+2)\ \ldots\ \underline{r}^T(k+H_p))^T$

$$\begin{aligned} J &= (\underline{r}_p - \underline{y}_p)^T \mathbf{Q}_p (\underline{r}_p - \underline{y}_p) + \tilde{\underline{u}}_p^T \mathbf{R}_p \tilde{\underline{u}}_p \\ &= (\underline{r}_p - \mathbf{A}_p \underline{x}(k) - \mathbf{B}_p \tilde{\underline{u}}_p)^T \mathbf{Q}_p (\underline{r}_p - \mathbf{A}_p \underline{x}(k) - \mathbf{B}_p \tilde{\underline{u}}_p) + \tilde{\underline{u}}_p^T \mathbf{R}_p \tilde{\underline{u}}_p \quad . \end{aligned} \tag{8}$$

The block diagonal matrices $\mathbf{Q}_p$ and $\mathbf{R}_p$ consist of $\mathbf{Q}$ and $\mathbf{R}$ matrices from eq. (1) on the main diagonal if $H_1 = 1$. For $H_1 > 1$, the first entries in the main diagonal are zero. Equating $dI/d\tilde{\underline{u}}_p = \underline{0}^T$ as a necessary and sufficient condition for an extremum yields for the future control input

$$\tilde{\underline{u}}_p = (\mathbf{B}_p^T \mathbf{Q}_p \mathbf{B}_p + \mathbf{R}_p)^{-1} \mathbf{B}_p^T \mathbf{Q}_p (\underline{r}_p - \mathbf{A}_p \underline{x}(k)) \quad . \tag{9}$$

As no constraints are considered, a closed form of the control law is obtained. From $\tilde{\underline{u}}_p = (\underline{u}_f(k)\ \underline{u}_f(k+1)\ \ldots)$ only the first entry, i.e. $\underline{u}(k) = \underline{u}_f(k)$, is applied to the process. Then, the optimization starts from the beginning using the measurement $\underline{y}(k+1)$ to determine a new state $\underline{x}(k+1)$, and so forth. To obtain a state estimate, a model-based measuring technique such as a Kalman filter[13] has to be applied if the full state vector $\underline{x}(k+1)$ cannot be measured.

II.B.   Alternative formulations

An alternative formulation can be given starting from an input-output description of the system in the z-domain or applying the so-called shift operator q^{-1} to a time-series model. In such a case, no state appears in the formulas but historic values $\underline{y}_h$ and $\underline{u}_h$, see figure 1. An example will be given in the burner study below. However, for long prediction horizons a formulation in state-space is superior from a numerical point of view.

In the first example of a flow past a cylinder a nonlinear model in continuous time serves for prediction. It is solved numerically by a forth-order-Runge-Kutta scheme. State estimation is done employing an extended Kalman filter. Moreover, input constraints are considered as well. The optimization problem is solved numerically by applying the `lsqnonlin` routine from MATLAB®, i. e. by a nonlinear least squares method, for more details see[2]. For the reduction of the drag of a bluff body in the last example a linear state-space model is used. However, instead of u_f, changes in u_f are introduced in eq. (1).

American Institute of Aeronautics and Astronautics

III.   Results

(N)MPC will now be applied to different flow control problems using different model formulations. In the flow past a circular cylinder, see section III.A, a NMPC will clearly outperform the best controller found in previous simulation studies[26]. Section III.B summarizes first results of the damping of Tollmien-Schlichting waves exploiting a Galerkin approximation. The last two sections, III.C and III.D, are devoted to experimental MPC-studies for a burner and a bluff body, respectively.

III.A.   2D flow around a circular cylinder

The present case study focuses on the two-dimensional laminar flow around a circular cylinder, see figure 2. The Reynolds number Re is chosen well above the critical Reynolds number 47, see,[?] for the onset of 2D
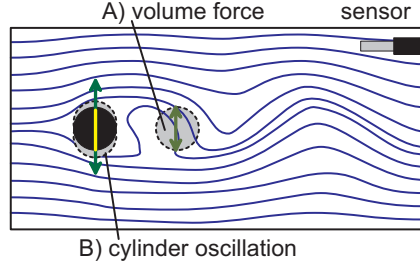

Figure 2. Principal sketch of the actuated cylinder wake. The figure displays the streamlines of the natural flow around a circular cylinder with diameter $D = 1$ (solid circle). Actuation is provided by transverse cylinder oscillation or by a transverse volume force in the grey circle. The flow state is sensed with a hot-wire anemometer, located at a typical position. Success of control is monitored in the observation region $-5 < x < 15$, $-5 < y < 5$, with $x = y = 0$ in the center of the cylinder, see figure 4 as well.

vortex shedding and well below the 3D instability around 180. The control goal is to suppress the stable 2D vortex shedding at that Reynolds number.

III.A.1.   Galerkin model for predicting the future development

A Karhunen-Loève (KL) decomposition of the unactuated flow shows that 96% of the turbulent kinetic energy E can be resolved with the first 2 KL modes, see[18] and[34]. To describe the transient from the (unstable) steady state solution, $\boldsymbol{U}_s$, of the Navier-Stokes equation (NSE) to the vortex shedding mode, $\boldsymbol{U}_i$, $i = 1, 2$, a third so-called shift mode $\boldsymbol{U}_\Delta$ has to be included in the Galerkin approximation as a key enabler for a successful approximation[34]. $\boldsymbol{U}_\Delta$ accounts for the difference between the mean and steady flow. With these 3 modes, a Galerkin approximation reads

$$\boldsymbol{U}(x, y, t) = \boldsymbol{U}_s(x, y) + \sum_{i=1}^{2} a_i(t)\boldsymbol{U}_i(x, y) + a_3(t)\boldsymbol{U}_\Delta(x, y) \tag{10}$$

in which $\boldsymbol{U}(x, y, t)$ describes the space- and time-dependent 2D velocity profile. For more details see[34].

The term $a_1(t)\boldsymbol{U}_1(x, y) + a_2(t)\boldsymbol{U}_2(x, y)$ approximates the oscillatory fluctuation associated with the von Kármán vortex street due to a nearly sinusoidal behavior of the Fourier coefficients $a_1(t)$ and $a_2(t)$.

Two different actuators are sketched in figure 2, namely a transverse oscillations of the cylinder and a volume force. The second approach will be considered in this paper. A practical implementation may be done with a magneto-hydrodynamic force. The flow state is sensed with a hot-wire anemometer, located at a typical position, see figure 2. As a result, a SISO set-up with one input and one output is considered.

Including the volume force in the momentum equation leads to the following modified Navier-Stokes equation

$$\frac{\partial \boldsymbol{U}}{\partial t} + (\boldsymbol{U}{\cdot}\nabla)\boldsymbol{U} = -\nabla p + \frac{1}{Re}\triangle \boldsymbol{U} + \boldsymbol{b}u \quad . \tag{11}$$

The control input $u \in R^1$ describes the amplitude of the forcing on a compact support given by $\boldsymbol{b}$ in the area shown in figure 2. A Galerkin system as a low order model is derived by projecting the NSE onto the modes and then applying a Kryloff-Bogoliubov ansatz, see[34]. The resulting Galerkin system has a more

American Institute of Aeronautics and Astronautics

simple structure in polar coordinates. With $a_1 = A\cos\Phi$, $a_2 = A\sin\Phi$ the low order model is given by

$$\begin{bmatrix} \dot{A} \\ \dot{\Phi} \\ \dot{a}_3 \end{bmatrix} = \begin{bmatrix} (\sigma_r - \beta a_3)A \\ \omega + \gamma a_3 \\ \alpha A^2 - \sigma_3 a_3 \end{bmatrix} + \begin{bmatrix} g_c\,\cos\,(\Phi - \theta) \\ -(g_c/A)\,\sin\,(\Phi - \theta) \\ 0 \end{bmatrix} u \quad . \tag{12}$$

As a result, the state vector reads $\underline{x}(t) = (A(t)\ \Phi(t)\ a_3(t))^T$. It should be pointed out that the model parameters α, β, γ, σ_r, σ_3, ω, and g_c, are obtained from a projection from an open-loop reference simulation. This may impose a major challenge when a controller is employed in a Navier-Stokes simulation. The low dimensional model is only valid in the vicinity of the operating conditions which were used to derive the POD modes. To account for this limited validity, Gerhard et al.[18] suggested that the control should not drive the system too far away from the manifold described by eq. (12). To this end, they proposed a first nonlinear control law which is based on physical insight, see figure 3. In this control law a piece-wise constant control
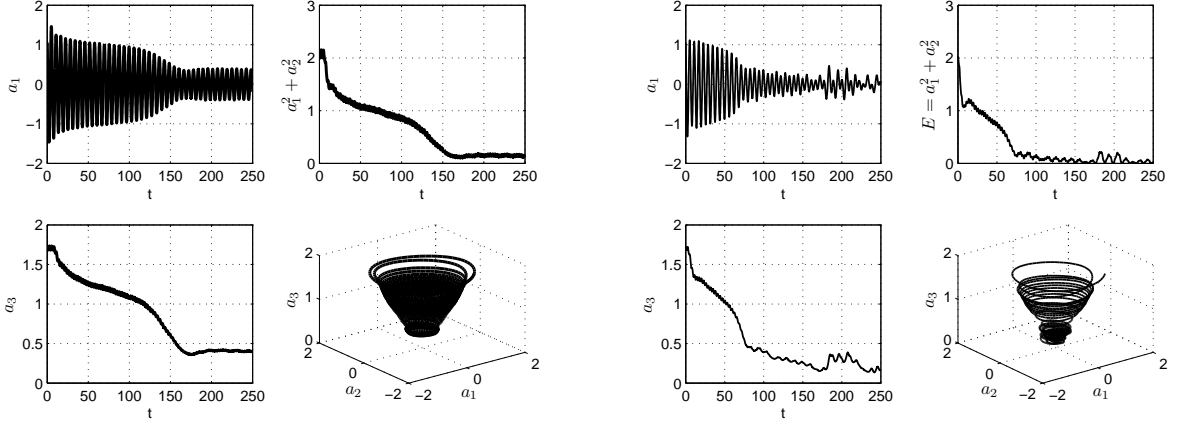

Figure 3. Fourier coefficients a_i obtained in a closed-loop controlled DNS by applying the controller based on physical intuition from[18] (left) and NMPC (right). State estimation is done with an extended Kalman filter. The success of the control is observed by $a_1^2 + a_2^2$ which describes the major part of the turbulent kinetic energy.

input u is applied. The magnitude of u is calculated such that the amplitude of the oscillation decreases, i.e. $\dot{A} < 0$, see eq. (12). Its sign is synchronized with $\cos\,(\Phi - \theta)$. By this, the mean impact on $\dot{\Phi}$ describing the harmonic vortex shedding is minimized, as the right hand side of this equation is shifted by $90°$ with respect to the control input. In King et al.[26] a simpler version of this control law was found and compared to different formally derived nonlinear controllers. Examples comprise input-output linearization, back-stepping, Lyapunov-based approach, etc. None of the formal methods could outperform the physically motivated controller which was named energy-based control. In a later improvement[2], back-stepping and Lyapunov-based approach resulted in better performances, though. However, as these methods are more involved, the energy-based controller will serve as a reference here.

To relax the problems coming from a limited validity of the model, an extended Kalman filter for state estimation will be implemented in the closed loop described below. By this, part of the model uncertainties can be accounted for when the system is driven away from the situation for which the POD modes were determined.

III.A.2.   *Closed-loop control*

For the well-known benchmark of the flow past a circular cylinder, a NMPC controller is build next. The prediction in the NMPC algorithm is based on eq. (12). As no experimental set-up is available, the obtained control law is tested in simulations studies using a direct numerical simulation. The simulations are performed on a grid with 8712 nodes. For state estimation based on the velocity measurement depicted in figure 2, an extended Kalman filter is applied. Details can be found in Aleksic et al.[2].

A very simple cost functional is used here instead of eq. (1)

$$J = \int_t^{t+H_p} e^2(l)dl \qquad \text{with} \qquad e(t) = r(t) - \hat{a}_1 \quad , \tag{13}$$

i.e. the control effort is neglected. The scalar reference $r(t)$ is chosen as a sinusoidal signal with exponentially decreasing amplitude. This choice is motivated by the limited validity of the low dimensional Galerkin system. The variable $\hat{a}_1(t)$ denotes the estimated value of the state variable $a_1(t)$. To make the optimization problem easier, we use even more physical knowledge about the process. From the physically motivated controller it is known that good results are obtained when a piece-wise constant u is synchronized with $cos(\Phi - \theta)$. This knowledge is exploited here as well. No arbitrary sampling period h, see figure 1, is chosen, but one that exactly matches the physics of the process. Inside a sampling period, u_f is chosen to be constant.

To respect the vaildity of the model, the calculated future control inputs are constraint to $|u_f(t+l)| < 0.1$. For more details see[3]. A comparison in figure 3 shows the superiority of NMPC which is much faster than energy-based control and leads to a recirculation zone of length 5.2 in contrast to 4.1 for the energy-based control. With no other controller using the very same measurement information and the same actuation concept such good results were found in King et al.[26]. Even with the improved versions of the backstepping and Lyapunov-based controllers in[2], a poorer performance was obtained. Figure 4 shows a plot of the streamlines of the unactuated and the actuated case with the NMPC controller at t=165. The damping effect of the actuation and the significant mitigation of the instability is clearly visible in the observation region.
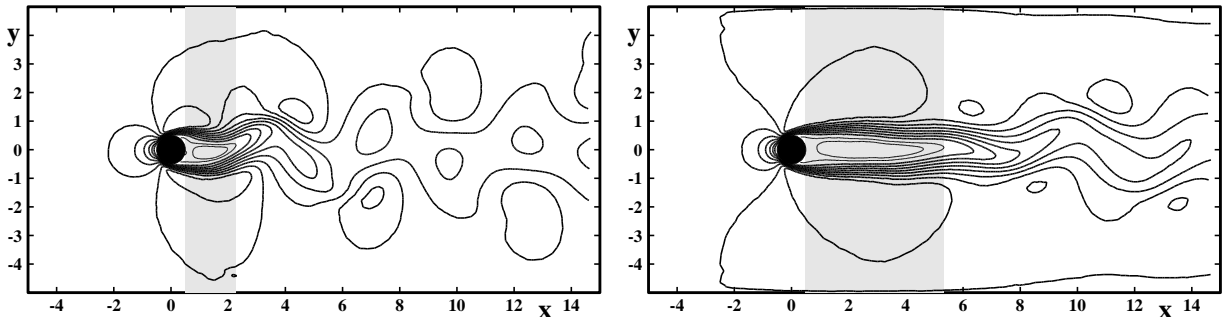

Figure 4. Left: Unactuated flow. Right: Actuated flow with an NMPC controller shown for $t = 120$. The figures display isocontours of the stream-wise velocity component U. Negative values are indicated by thinner curves and show the extent of the recirculation region.

III.B.   Damping of Tollmien-Schlichting waves

The final goal of this study will be the damping of Tollmien-Schlichting (TS) waves to delay transition from a laminar to a turbulent regime. Sturzebecher and Nitsche[43] performed an active cancellation of Tollmien-Schlichting (TS) instabilities on a wing using multi-channel sensor actuator systems to delay transition. The control law is based on a high order filtered x-LMS method. With an error and a reference sensor a control input is calculated such that at the location of the error sensor a significant mitigation of the TS waves is obtained, see as well Wu and Breuer.[46] Evert et al.[14] use a nonlinear black-box model based on Volterra filters for the same purpose. A similar attenuation of the instability in an experimental wind-tunnel test can be obtained using a significantly simpler approach. In this case, experiments with extremum seeking control - which was roughly explained in section I - give rise to an attenuation of the *rms*-value of surface hotwire measurements of $> 60\%$ when artificial TS waves are introduced (unpublished results).

In this study, damping will be performed either by synthetic jet actuators or by actively controlled flexible walls. With both set-ups, first promising results are obtained in experiments. When stacked synthetic jet actuators are used, sensors can be placed in between a pair of actuators, whereas in the case of a flexible wall measurements are possible only in front and after the flexible wall segment. This latter more difficult situation will be considered in the following. As true TS waves appear in packets (which we are able to detect) and as these packets consist of TS waves with a spectrum of different frequencies, these first investigations will focus on a more simple situation. By artificially introducing harmonic pertubations in an upstream section, e.g., by a synthetic jet actuator as well, a continuous TS wave with a fixed frequency is triggered.

Concerning the application of MPC to dampen TS waves only preliminary results can be given here. Therefore, only simulation studies are considered. The simulation is performed with a two dimensional DNS solver, see Rist and Fasel[40] and[27]. This solver computes the flow on a 850x90 rectilinear grid over an area of 0.683865 to 4.6399 non-dimensional units in x and 0 to 0.0956 in y. This corresponds to a displacement-thickness Reynolds-number of 450 to 1180 in x. It is assumed that a wall-normal velocity can be measured

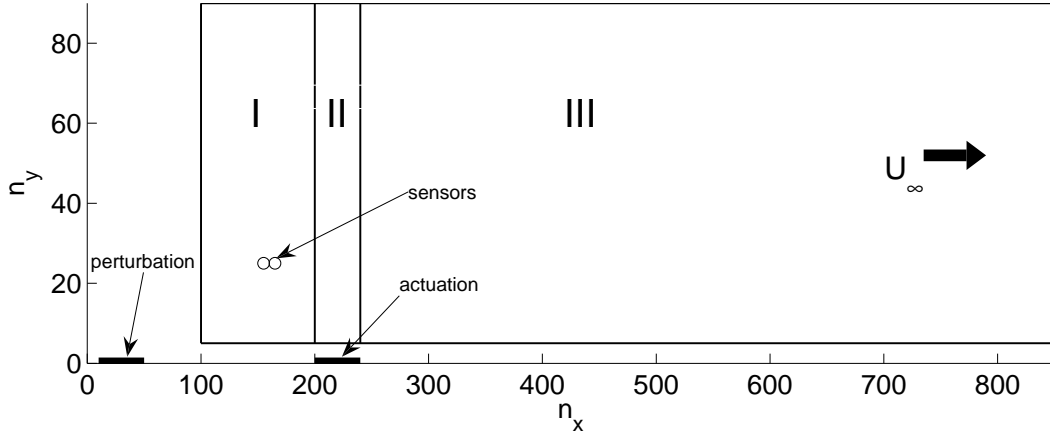American Institute of Aeronautics and Astronautics

Figure 5. Domains considered for the damping of TS waves. Subregions I,II and III are used for POD and Galerkin-projection. A black-box model is identified for the effect of actuation on subregion II. x represents streamwise, y wall-normal direction.

at the locations given in figure 5. The y position is chosen for ease of calibration, as this is the v-velocity profile's maximum. In experiments, however, it was already shown that TS waves can be estimated as well with surface hotwires (unpublished results).

In the actuation strip, i.e. subregion II, the boundary value of the wall-normal velocity is set by a controller. This has a similar effect as a wall displacement, as the flow reacts to the velocity profile prescribed at the wall. The wall velocity profile in streamwise direction in the actuation strip, see figure 5, is restricted to a half-sine as function of x with a time-variable amplitude to match membrane displacements in later experiments. In the perturbation region upstream, disturbances are seeded to trigger artificial TS waves. This is done by setting appropriate boundary conditions.

III.B.1. Galerkin model for predicting the future development

A Galerkin approximation of the 2D flow over a flat plate is used similar to the circular cylinder study shown before to derive a low dimensional model. A major challenge in creating the low dimensional Galerkin system is, as always, the inclusion of the control input. As modes $\mathbf{U_i}(\mathbf{x}, \mathbf{y})$, such as POD modes, describe global effects, the inclusion of a local actuation is difficult. To this end, a new approach is proposed here.

In a first step, POD modes are determined for the unactuated case for the whole region covering subregions I, II and III, see figure 5, when TS waves are triggered by the pertubation upstream. Note that the areas directly at the wall (5 closest DNS nodes) and close to the perturbation have been omitted from the POD because the wall region's steep gradients negatively affect the calculation of the Galerkin projection. Likewise, as clean TS waves are only developed some distance downstream of the pertubation strip, this part is not used either. Figure 6 displays the first two most energetic modes.

From the modes derived, a Galerkin projection is performed to obtain a Galerkin system describing the time evolution of the Fourier coefficients, see section III.A. These Fourier coefficients will be named $a_i^{(u)}(t)$ as they are obtained from an unactuated situation. The resulting Galerkin system is further modified using physical insight to offset numerical errors. For example, the production terms calculated by the projection are set to zero, as they only arise from numerical errors. As no actuation is used in the snapshots from which the modes are derived, this Galerkin system describes the evolution of the unactuated flow's Fourier coefficients describing TS waves only.

In the next step, different actuation signals $u(t)$ are applied in the simulation. This simulation will yield experiments for a system identification. It is performed without triggering TS waves with the upstream pertubation. The obtained snapshots of the velocity profile of the flow are then projected onto subregion II of the modes found in the first step. This projection resulting in actuated Fourier coefficients $a_i^{(a)}(t)$ is only done in subregion II, as no upstream effect of the actuation can be observed, and the downstream effect outside the actuation area is convective. Thus, we concentrate on the effect on subregion II.

Now, system identification methods are used to derive a black-box model describing the relation between

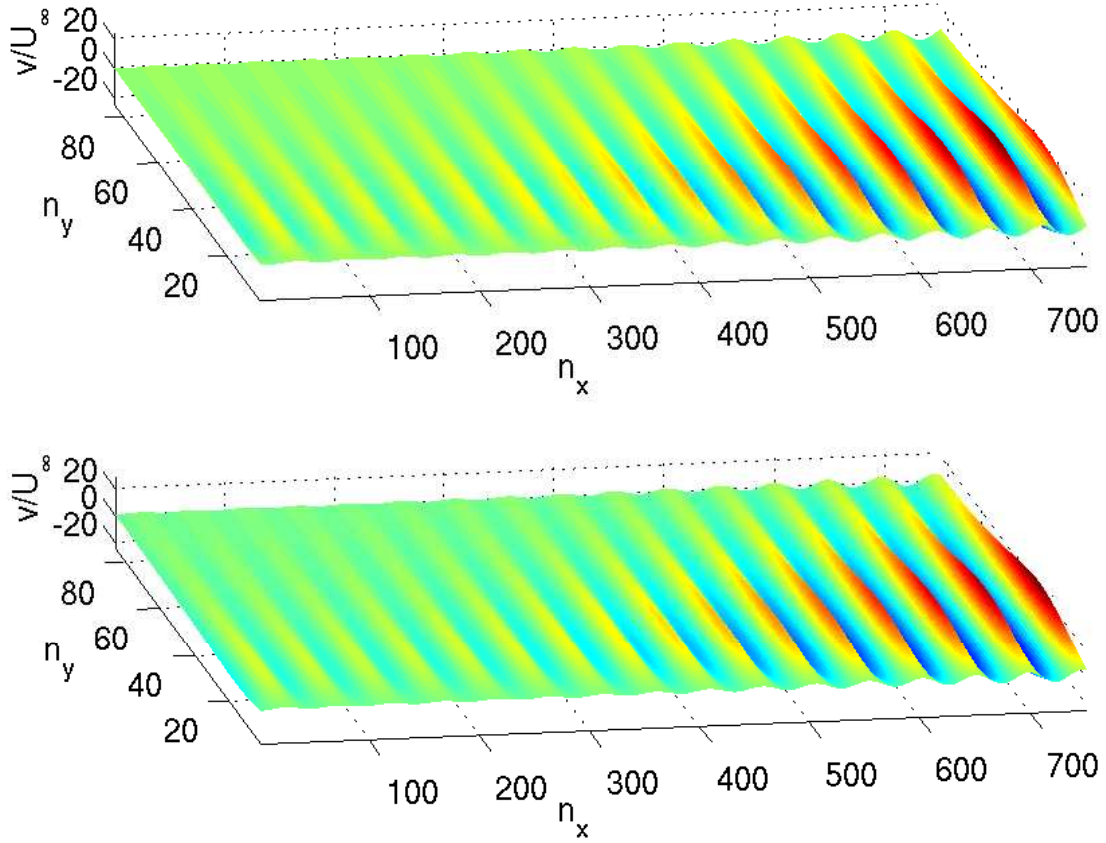American Institute of Aeronautics and Astronautics

Figure 6. Most energetic POD-modes for the flow over a flat plate. The normalized wall-normal velocity component is shown as a function of the streamwise and wall-normal computation nodes for subregions I, II and III, i.e. excluding the 5 closest DNS nodes to the wall. A non-equidistant spacing is used for the nodes.

applied control input $u(t)$ and the time evolution of the first two actuated Fourier coefficients $a_1^{(a)}(t)$ and $a_2^{(a)}(t)$. It should be noted that still the same POD modes are assumed to be valid, even though only a 'local' part of them is used. Thus, the derived effect on the coefficients is also only local. A state-space model is identified using a prediction error method from the MATLAB® system identification toolbox.

If TS waves are triggered upstream by the pertubation and an actuation signal $u(t)$ is applied in the actuation region at the same time, the overall Fourier coefficients obtained for subregion II are given by a superposition, i.e. $a_i(t) = a_i^{(u)}(t) + a_i^{(a)}(t)$. This is confirmed by simulation studies. Hence, a combination of the two models, Galerkin system and black-box model, can be used to estimate the flow state in the actuation region. To improve this estimation, the state of the Galerkin system is corrected by an extended Kalman filter using the two sensors in subregion I.

Based on an actual estimate of the flow state, a prediction of the future development is calculated next. In the uncontrolled case, the Galerkin system, i.e. $a_i^{(u)}(t)$, describes how this future evolution would look like. Theoretically, the negative value of this trajectory $a_i^{(u)}(t)$ could be used as a reference input $r(t)$ for the black-box model. If a model predictive controller is now able to synthesize a control input $u(t)$ such that the response of the actuated system $a_i^{(a)}(t)$ equals the negative value of the unactuated case, a superposition would lead $a_i(t) = 0$. However, such an approach would not be physical. Therefore, $r(t) = -Ka_i^{(u)}(t)$ is chosen with a small K, e.g. $K = 1/65$.

Based on this idea, a MPC scheme is build. The presented results are for a prediction and control horizon $H_p = 5$, $H_c = 1$, respectively.

Using this control scheme, the amplitude of disturbance of the flow can be reduced by $> 80\%$ at $x/dx =$
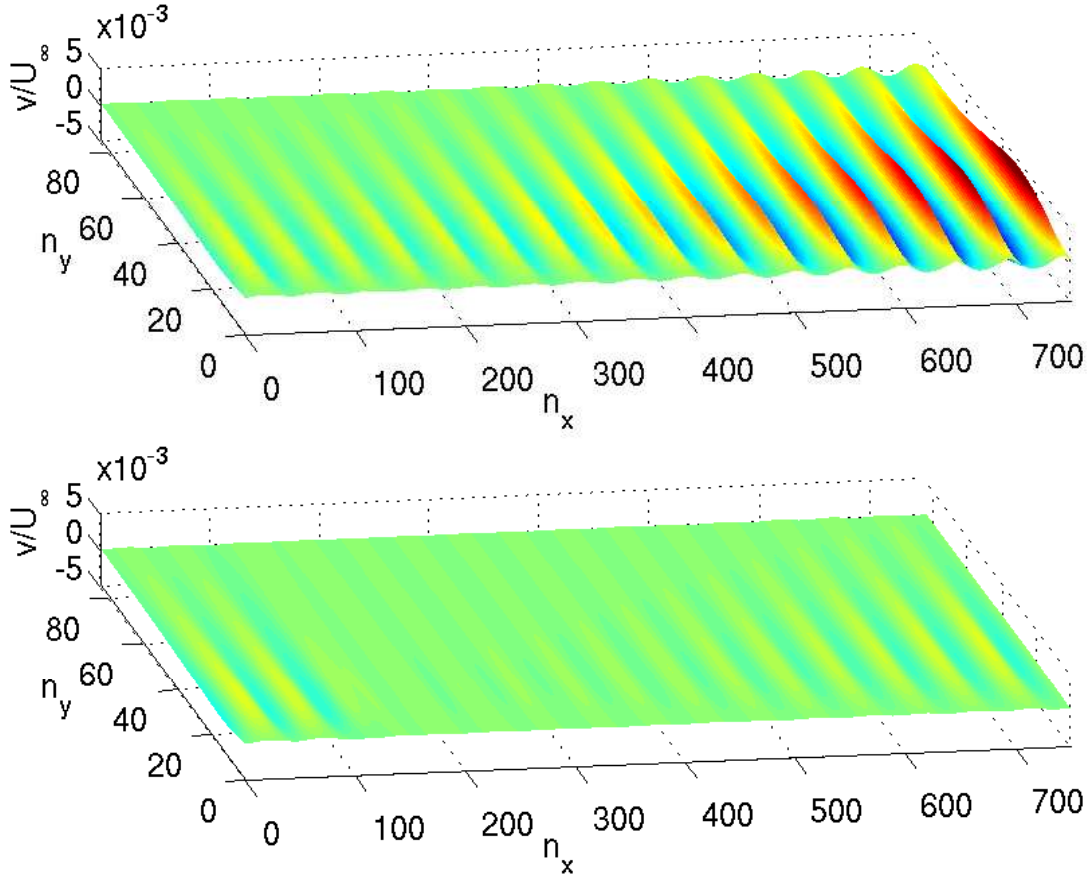
Figure 7. Snapshot of the disturbance velocity field without (top) and with actuation (bottom), see figure 6 for more explanations.

850 (see figure 7). This value could be further increased by matching the actuation profile perfectly to the wavelength of the TS waves, but this was not the focus of this study. Rather, it is shown that MPC can be used for TS waves even without perfect actuators or measurements in the actuated region.

III.C. Control of thermoacoustic instabilities in a burner

Lean-premixed combustion offers a way to meet restrictive, low emission levels for modern gas turbines. However, the leaner a combustion system operates the more it is prone to suddenly occurring large pressure oscillations[11, 28, 37]. These so-called thermoacoustic instabilities arise from the interaction of unsteady heat release and the acoustic field in the engine. If the two mechanisms interfere with an unfavorable phase relation, high amplitude pressure pulsations occur, which have a detrimental effect on the combustion process.

Active control can be used to suppress thermoacoustic instabilities. Model-based closed-loop control of combustion instabilities was shown to be effective in reducing the pressure oscillations considerably. Morgans and Dowling[31], e.g., used Nyquist techniques to build a stabilizing controller. The simplest form of closed-loop control is a phase-shifted pressure feedback by the so-called phase-shift or time-delay controller[12]. Here, the combustor pressure is fed back via acoustic or fuel modulating actuators. In the Laplace domain the control law reads $C(s) = Ke^{-s\tau}$ (K being the gain and τ the delay). The two control parameters K and τ are either tuned empirically or optimized by an adaptive scheme[5, 30].

The combustor test rig considered in this investigation is shown schematically in figure 8. A swirl-stabilized burner, generating an aerodynamically stabilized flame, is mounted in a cylindrical silica glass combustion chamber. The usual operating range comprises equivalence ratios from $\phi = 0.5$ to stoichiometric level and a thermal power of about 80-240 kW. Several 1/4" condenser microphones are mounted up- and
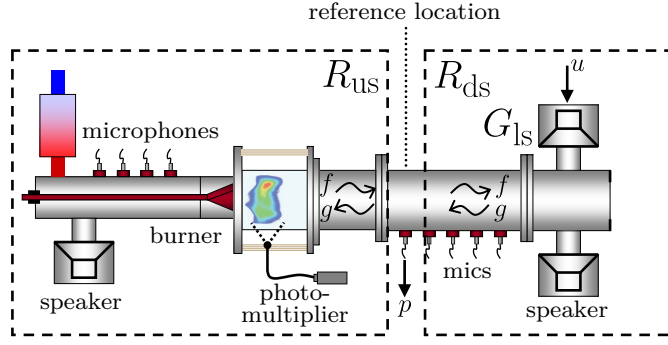
Figure 8. Schematic of the test rig set-up. Linear sub-models $R_{us}(s)$, $R_{ds}(s)$ and $G_{ls}(s)$ are identified for the dashed upstream and downstream box and the actuator, respectively.

downstream of the burner to allow for the decomposition of the plane acoustic field. More information is given in Gelbert et al.[17]. For model identification and control, actuation is provided acoustically by speakers mounted up- and downstream of the flame.

III.C.1. *Black-box model for predicting the future development*

The mathematical model used in the following linear MPC algorithm is exclusively based on input/output data. For this, the combustion system is divided into an upstream and a downstream part, as shown in figure 8. The acoustic characteristics of each part are represented as complex reflection coefficients R_{us} and R_{ds}, relating the reflected to the incident plane acoustic wave in the frequency domain. These two parts are identified with system identification methods from pressure signals obtained when a one-sided actuation through a loudspeaker is applied. For identification, chirp signals are used. More details about this non-trivial identification of an unstable plant can be found in Gelbert et al.[17] and the references therein. Actuation is taken into account by modeling the left traveling wave $g(s)$ of the downstream part as in Bothien et al.[9] by a part which is a result of the reflected right traveling wave $f(s)$ and another part coming from the control input $u(s)$

$$g(s) = R_{ds}(s)f(s) + G_{ls}(s)u(s) \quad . \tag{14}$$

G_{ls} is the actuator transfer function and $u(s)$ is the manipulated variable in the Laplace domain, respectively. State space matrices, as introduced in section II, relate to the transfer functions in the Laplace domain according to $G(s) = \mathbf{C}(s\mathbf{I} - \mathbf{A})^{-1}\mathbf{B}$ if a continuous representation is chosen. Combining Eq. (14) with the relations for the upstream reflection coefficient, $f(s) = R_{us}(s)g(s)$, and for the pressure, $p(s) = f(s) + g(s)$, leads to the total plant transfer function $G_s(s)$,

$$p(s) = G_s(s)u(s) = G_{ls}(s)\frac{1 + R_{us}(s)}{1 - R_{ds}(s)R_{us}(s)}u(s) \quad . \tag{15}$$

Equation (15) relates the scalar input command $u(s)$ to the scalar output $y(s)$ which equals the pressure $p(s) = y(s)$ at a reference plane (see figure 8). Hence, a SISO problem is considered again. A Bode plot, i.e. $|G_s(j\omega)|$ and $\arg\{G_s(j\omega)\}$ as a function of ω, is shown in figure 9 (left).

The MPC algorithm has to be implemented in a discrete-time fashion on a rapid prototyping hardware (dSpace® DS1103-PPC controller). Therefore, a discrete-time version of eq. (15) written as a time-series model is exploited in the form

$$p(k+1) = -a_0 p(k) - a_1 p(k-1) - \cdots - a_{na}p(k-na) + b_0 u(k-d) + b_1 u(k-d-1) + \ldots b_{nb}u(k-d-nb) \tag{16}$$

in which d is a time-delay in the general case. As the absolute value of poles of discrete transfer functions tends to move closer to 1 when the sampling frequency is increased, numerical problems occur with the discrete model if too large sampling frequencies are chosen. Therefore, the sampling frequency is set to 1000 Hz. In future implementations, a formulation with a discrete-time state-space description as outlined in section II will be used instead. Then, sampling frequencies of 3000 or more Hz will be possible. Details about the actually implemented algorithm can be found in Gelbert et al.[17].

As this thermoacoustic system and the identified model are unstable, a prediction of the future development of the plant is likely to lead to numerical problems in the MPC algorithm, irrespective of the formulation
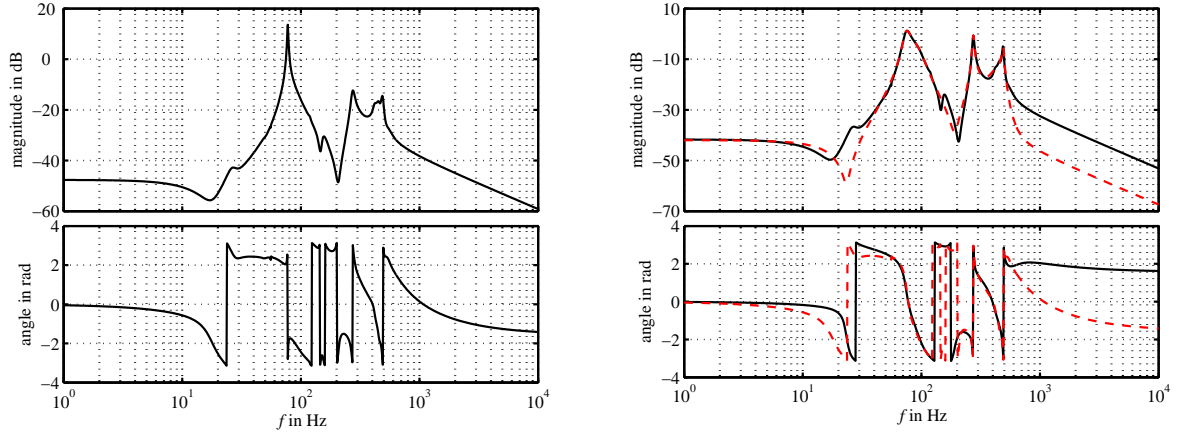
Figure 9. Bode diagrams of identified systems. Left: Transfer function G_s of the plant to be controlled. Right: Stabilized system G_c (black solid) and reduced order model of order 10 (red dashed).

whether in state-space or in the z-domain. Therefore, two control loops are build up. In an inner loop the aforementioned phase-shift controller $C(s)$ stabilizes the system, see figure 10. The location of the reference pressure sensor is chosen such that a time-delay $\tau = 0$ results, i.e. $C(s) = K$. The MPC algorithm then determines the set-points u_{mpc} for this inner loop. As a consequence, the model used in the MPC is not
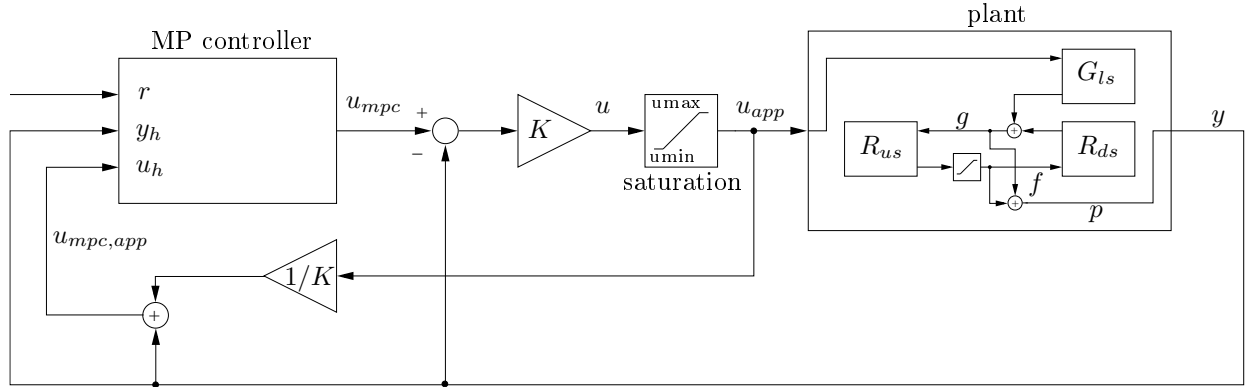

Figure 10. Cascade-like implementation of the MP controller for a single input single output problem.

$G_s(s)$, but

$$G_c = \frac{KG_s}{1 + KG_s} \qquad . \tag{17}$$

This leads to a transfer function of order $na = 40$. To simplify the calculations in the MPC algorithm, a reduced order model with a similar frequency response in the frequency range of interest is determined. The Bode plot of G_c and the reduced model of order 10 can be seen in figure 9 (right) as well.

The output of the MP controller, denoted by u_{mpc} in figure 10, equals the first control move of the MPC algorithm, i.e. $u_{mpc} = u_f(k)$.

As in section II, an unconstrained optimization is solved again giving rise to an explicit formula to calculate the next control move. However, when the next output of the MPC algorithm u_{mpc} is processed by the inner loop, a violation of physical constraints with respect to the loudspeaker input signal u may appear through $u = K(u_{mpc} - y)$. These input signals are therefore limited in an ad hoc fashion by an implemented saturation block to $-0.9\text{V} < u < 0.9\text{V}$, see figure 10. A better way to account for such constraints would be an inclusion into the optimization problem which will be part of future work. In the algorithm implemented, as well old values of the control input (and output) occur, as it is based on a description as shown in eq. (16). To account for a saturated input to the loudspeaker u_{app} in the next prediction, this information is given to the MPC algorithm as well, see figure 10. More details can be found in[17]. Using a state-space based MPC, a correction would only be necessary in the Kalman filter. Here, all past information is contained in

American Institute of Aeronautics and Astronautics

$\underline{x}(k)$.

III.C.2. Closed-loop control

The test rig is operated with natural gas at an equivalence ratio of 0.62 and a thermal power of 110 kW. This operating condition causes a high amplitude thermoacoustic instability, see figure 11(a), black, where the acoustic pressure is shown. Distinct peaks at 81 Hz and its harmonics can be seen. This oscillation frequency corresponds to the $\lambda/4$-mode of the test rig. Peak amplitudes of 155 dB are observed.
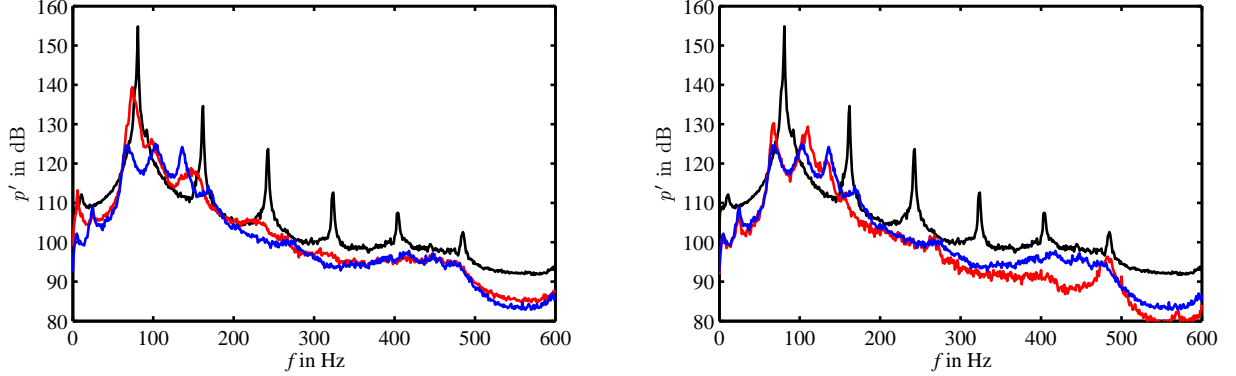
(a) Comparison of the proportional control (red) with the un-weighted MPC (blue); baseline case without control (black).

(b) Comparison of the weighted MPC (red) with the un-weighted MPC (blue); baseline case without control (black).

Figure 11. Spectra of acoustic pressure

Suppression of the instability with a simple proportional controller results in a peak amplitude attenuation of approximately 16 dB (red line in fig. 11(a)). The peak amplitude is still quite high but no harmonics are present anymore. Applying the MPC (blue), it is possible to achieve a significantly higher reduction. The peak amplitude is decreased by 31 dB, i.e. to less than 3 % of its initial value. However, higher harmonics show up which may be a result of a spill-over effect resulting in peak-splitting, see as well[6].

An unweighted MP controller is used here with respect to the control error $r - y$, i.e. $\mathbf{Q_p} = \mathbf{I}$ and $\mathbf{R_p} = \mathcal{O}$, which means that the control input is not penalized. To account for dead-times and to improve the closed-loop behavior the summation in the first term in eq. (1) starts from $H_1 = 40$. The prediction horizon is set to $H_p = 150$. Only one control move is allowed in the MPC, i.e. $H_c = 1$.

A typical experiment with this controller is shown in figure 12(a) (top). High pressure fluctuations are observed in the beginning when the control is off. At $t \approx 7$ s, the proportional controller is switched on. The fluctuations are slightly mitigated. The proportional controller is then switched off and on again (black in fig. 12(a), bottom). Starting from $t \approx 37$ s, the cascaded MPC-scheme using an inner proportional controller is used. A further reduction in the amplitude of the acoustic pressure compared to the proportional controller results.

Since the control signal u_{mpc} is not weighted at all, large control commands u_{app} are applied to the plant (see fig. 12(a) middle). Figure 12(b) shows a magnification of the applied control variable u_{app} (black) and the control variable u_{mpc} (red) during control with the unweighted MP controller. Obviously, u_{app} is saturated only slightly.

During the control with the proportional controller, the control variable u_{app} does not exceed 0.6 V. It should be noted that a further increase of the control gain does not cause a further decrease of the oscillation amplitude. Increasing the gain beyond a certain threshold even results in an amplification of the instability.

In order to avoid u being saturated by the amplifiers' input limitation, a weighted MP controller ($H_p = 150$, $H_c = 10$, $H_1 = 20$, $\mathbf{Q_p} = \mathbf{I}$ and $\mathbf{R_p} = \mathrm{diag}(0.1)$) is applied next. Additionally, the changes in the control moves, i.e. $u(k + j + 1) - u(k + j)$ are penalized as well with the same weight $\mathbf{R_p}$, see[17]. The spectrum of the acoustic pressure fluctuations corresponding to this case is shown in red in figure 11(b). The black and blue lines are equal to the ones shown in figure 11(a), i.e. they represent the baseline case and the result of MPC without weighting. The system is still stabilized, however, the resulting attenuation of 25 dB of the peak amplitude is slightly less than in the case without weighting. On the other side the spectra 13(a) and the time traces 13(b) of the control input show that the weighted MPC (in red) uses much less actuation

American Institute of Aeronautics and Astronautics
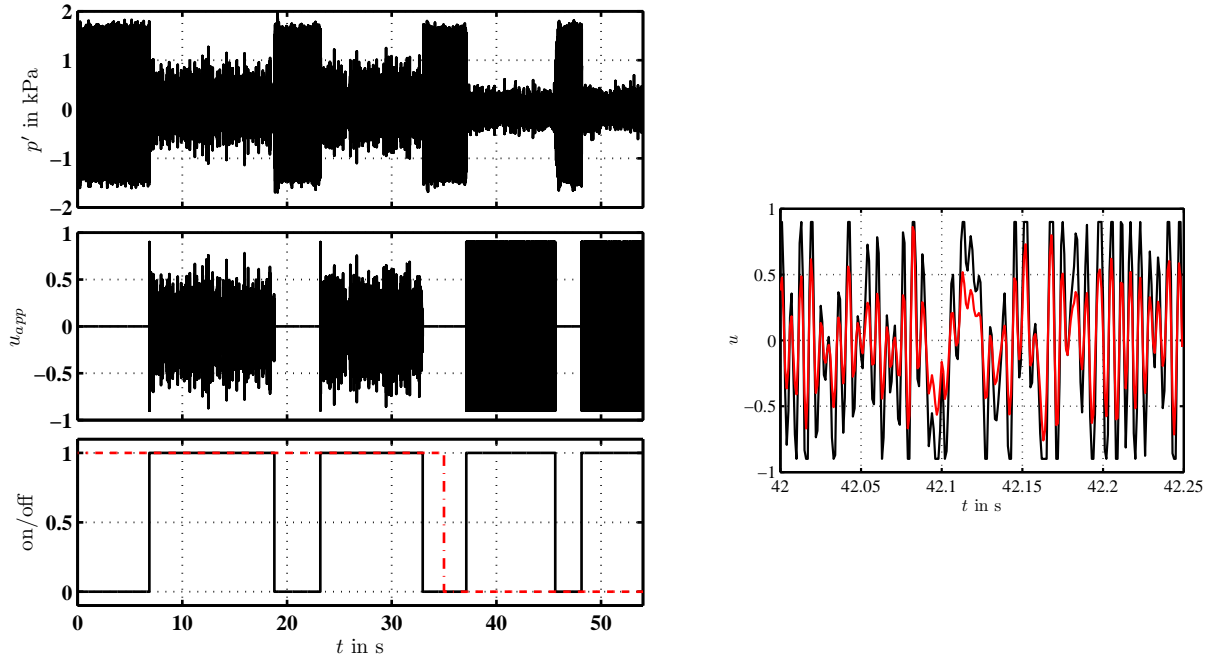
(a) Top: Pressure fluctuation; middle: actually applied control signal u_{app}; bottom: control on/off (black solid), 1-proportional control, 0-MP control (red dashed).

(b) Calculated control signal from the unweighted MPC u_{mpc} (red) and resulting signal driving the woofers u_{app} (black).

Figure 12. Time traces of the closed loop.

power compared to the unweighted MPC (in blue).

(a) Spectra of calculated control signals

(b) Section of the control signals' time responses
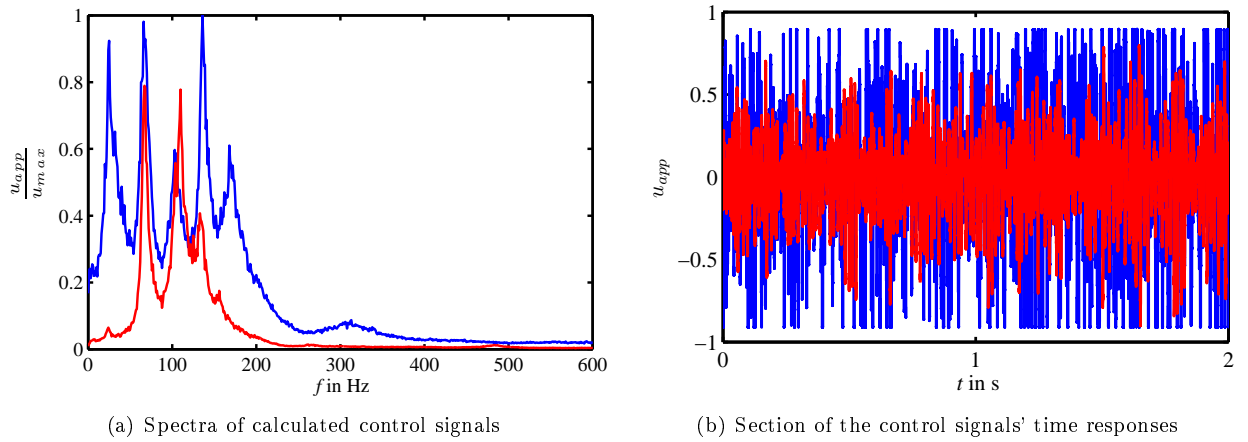
Figure 13. Comparison between weighted (red) and unweighted (blue) MPC.

III.D.   Reduction of the drag of an Ahmed body

In a companion paper by Muminovic et al.[32] a robust and a model predictive control of the flow past a 3D bluff body is discussed and compared extensively. An Ahmed body of 1/4 of the original size proposed by Ahmed[1] is considered in[32] with a constant blowing through two corner actuators. In this contribution, we show that the MPC algorithm can as well be applied to the full-scale Ahmed body. Different actuators and a harmonic actuation are used here. A sketch of the experimental set-up is given in figure 14. The experiments are conducted in a wind tunnel with a closed test section (cross section area $A_{TS} = 2.82\ m^2$, length $l_{TS} = 10\ m$). The free-stream velocity is $u_\infty = 7\mathrm{m/s}$. The shape of the generic car model is based on

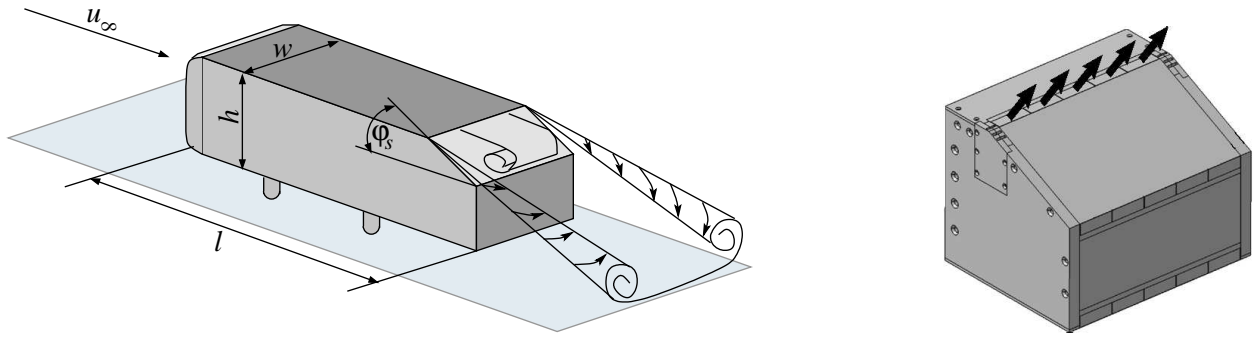American Institute of Aeronautics and Astronautics

Figure 14. **Left: Sketch of the Ahmed Body. Right: Rear part of the Ahmed body.** *Dieses Bild muss noch bearbeitet werden...*

the original geometry of the Ahmed body[1] (length l = 1044 mm, height h = 288 mm, and width w = 389 mm) with a slant angle $\varphi_s = 25°$ (see figure 14 left).

For blowing, cavities are integrated spanwise between the intersection of the roof of the body and the slant at the rear end (see figure 14 right). Periodic excitation is applied. The actuation frequency is set constant to a value of 60 Hz. The blowing forcing intensity is adjustable through a valve. Three more actuators are included in the model at the rear corners. However, only results for actuation with the actuator between the roof and the slant are shown here. A total of 27 pressure sensors on the slant and 9 on the base of the rear end are installed. Since it is assumed that the flow configuration is symmetric, the sensors are placed on one side of the body only. Each pressure reading is described by the non-dimensional coefficient

$$c_p(x, y, z, t) = \frac{\Delta p}{\rho \cdot u_\infty^2 / 2} \quad , \tag{18}$$

in which Δp is the instantaneous pressure difference between a stern-mounted pressure gauge and a reference pressure, and ρ denotes the density. A six component force balance mounted below the wind tunnel test section is used to measure the effect of the applied flow control method on the over all drag of the Ahmed body. Data acquisition and implementation of the controller is realized by a rapid prototyping hardware (dSpace® DS1103-PPC controller) with a sampling frequency of 350 Hz.
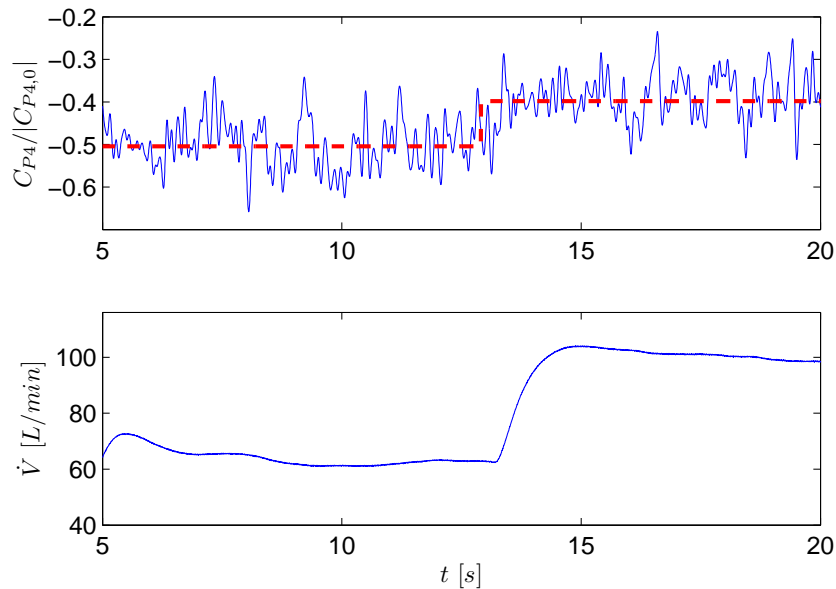

Figure 15. **Reference tracking experiment conducted at a Reynolds number of** $Re_l = 500000$. **Upper panel: Solid line represents the measurement, i.e. the normalized pressure coefficient at sensor position 4. The dashed line indicates the reference trajectory. Lower panel: Blowing intensity.**

Brunn et al.[10] showed that through the shape induced separation longitudinal and spanwise vortices

American Institute of Aeronautics and Astronautics

occur. These vortices impose a low pressure at the rear end of the Ahmed body. The resulting pressure difference between the front and the rear end is the main contributor to the overall drag. A good correlation between the sensor readings at sensor position 4 (located at the middle of the slant in the symmetry axis) and the overall drag exists. The aim of this investigation is to influence these vortices through periodic blowing in such a way that the pressure at the rear end increases and the overall drag decreases, as was shown in Brunn et al.[10].

For predicting the future behavior inside a MPC algorithm, a very simple first order model is identified from experiments, see as well[32]. In the Laplace domain it reads

$$G(s) = \frac{K}{T_1 s + 1} \quad , \tag{19}$$

and in discrete-time state-space form according to section II

$$\mathbf{A} = e^{-\frac{h}{T_1}} \quad , \quad \mathbf{B} = K T_1 e^{-\frac{h}{T_1}} (e - 1) \quad , \quad \mathbf{C} = 1 \quad . \tag{20}$$

The following parameters are chosen: $H_p = H_c = 1750$, i.e. 5 seconds, $\mathbf{Q_p} = \mathbf{I}$ and $\mathbf{R_p} = \text{diag}(10^{-7})$. Hence, the costs of the actuator signal are almost neglected.

Figure 15 presents a reference tracking experiment applying a linear MPC scheme. As can be seen, the MPC holds the normalized pressure coefficient at a constant level of -0.5. At approximately 13s, the value of the reference is changed. The MPC drives the system within 0.5s to the new reference level. The relatively slow dynamic is a result of a rather slow dynamical behavior of the valve used to regulate the blowing intensity. Otherwise, the MPC shows a good performance.

IV.   Conclusions

The more is known about a system, the better the control can be. In many classical controllers, models of a process are only used during synthesis of the controller. In contrast, MPC exploits a process model inside the algorithm. As an optimization problem over a future horizon is considered, there are no restrictions concerning the variables which are used to describe the success of control as long as they can be calculated by that model. Very different criteria can be formulated, combining different aspects at the same time. Moreover, when enough computing power is available, equality and inequality constraints can be included in the optimization in a straightforward manner. With no other control technique this practically very important issue can be dealt with so easily.

This contribution reviewed first applications of MPC for flow control problems. For the flow past a circular cylinder a constrained nonlinear MPC outperformed other nonlinear control approaches. The suppression of thermoacoustic instabilities in a burner could be further improved by a linear MPC in comparison to a simple proportional controller proposed earlier. First studies of the drag reduction of an Ahmed body and the suppression of Tollmien-Schlichting waves show promising results as well.

Acknowledgments

References

[1]S. R. Ahmed, R. Ramm, and G. Faltin. Some salient features of the time-averaged ground vehicle flow. In *SAE-paper 840300*, 1984.

[2]K. Aleksic, R. King, B.R. Noack, O. Lehmann, M. Morzynski, and G. Tadmor. Nonlinear flow control using a low dimensional galerkin model. In *X Triennial International SAUM Conference on Systems, Automatic Control and Measurements*, Nis, Serbia, 2007.

[3]K. Aleksic, R. King, B.R. Noack, O. Lehmann, M. Morzynski, and G. Tadmor. Nonlinear model predictive control based on a low dimensional model of fluid flow. In *Int. Conf. on Jets, Wakes and Separated Flows 2008*, Berlin, Germany, 2008.

[4]K.B. Ariyur and M. Krstic. *Real-Time Optimization by Extremum-Seeking Control*. John Wiley & Sons, Hoboken, 2003.

[5]A. Banaszuk, K. B. Ariyur, and M. Krstić. An adaptive algorithm for control of combustion instability. *Automatica*, 40:1965–1972, 2004.

[6]A. Banaszuk, Y. Zhang, and C.A. Jacobson. Active control of combustion instabilities in gas turbine engines for low emissions. Part II: Adaptive control algorithm development, demonstration and performance limitations. In *AVT Symposium on Active Control Technology for Enhanced Performance Operation Capabilities of Military Aircraft, Land Vehicles, and Sea Vehicles*, Braunschweig, Deutschland, 2000.

[7]J.-F. Beaudoin, O. Cadot, J.-L. Aider, and J.-E. Wesfried. Drag reduction of a bluff body using adaptive control methods. *Physics of Fluids*, 18:085107, 1–10.

[8]R. Becker, R. King, R. Petz, and W. Nitsche. Adaptive closed-loop separation control on a high-lift configuration using extremum seeking. *AIAA Journal*, 45:1382–1392, 2007.

[9]M. R. Bothien, J. P. Moeck, and C. O. Paschereit. Time domain modelling and stability analysis of complex thermoacoustic systems. *Proceedings of the Institution of Mechanical Engineers, Part A: Journal of Power and Energy*, 221(5):657–668, 2007.

[10]A. Brunn, E. Wassen, D. Sperber, W. Nitsche, and F. Thiele. Active drag control for a generic car model. In R. King, editor, *Active Flow Control*, volume 95 of *Notes on Numerical Fluid Mechanics and Multidisciplinary Design*, pages 247–259. Springer, Berlin, Heidelberg, 2007.

[11]S. M. Candel. Combustion instabilities coupled by pressure waves and their active control. In *24th Symposium (International) on Combustion*, pages 1277–1296. The Combustion Institute, 1992.

[12]A. P. Dowling and A. S. Morgans. Feedback Control of Combustion Oscillations. *Annual Review of Fluid Mechanics*, 37(2):151–182, 2005.

[13]A. Gelb (Ed.). *Applied optimal estimation*. MIT Press, 1974.

[14]F. Evert, D. Ronneberger, and F.-R. Grosche. Application of linear and nonlinear adaptive filters for the compensation of disturbances in the laminar boundary layer. *ZAMM*, 80(Suppl. 1):85–88, 2000.

[15]H.J. Ferreau, P. Ortner, P. Langthaler, L. del Re, and M. Diehl. Predictive control of a real-world diesel engine using an extended online active set strategy. *Annual Reviews in Control*, 31(2):293–301, 2007.

[16]M. Gad-el-Hak, A. Pollard, and J.-P. Bonnet, editors. *Flow Control: Fundamentals and Practices*. Springer-Verlag, Berlin, 1998.

[17]G. Gelbert, J.P.Moeck, M.R. Bothien, R. King, and C.O. Paschereit. Model predictive control of thermoacoustic instabilities in a swirl-stabilized combustor. In *Proc. of the 46th AIAA Aerospace Sciences Meeting and Exhibit*, 2008.

[18]J. Gerhard, M. Pastoor, R. King, B.R. Noack, A. Dillmann, M. Morzyński, and G. Tadmor. Model-based control of vortex shedding using low-dimensional Galerkin models. In *AIAA-Paper 2003-4262*, 2003.

[19]M.N. Glauser, H. Higuchi, J. Ausseur, and J. Pinier. Feedback control of separated flows. *AIAA-Paper 2004-2521*, 2004.

[20]T. Heine, M. Kawohl, and R. King. Model based estimation and optimal control of fed-batch fermentation processes for the production of antibiotics. *Chemical Engineering and Processing 46*, pages 1223–1241, 2007.

[21]L. Henning, G. Feuerbach, R. Muminovic, A. Brunn, W. Nitsche, and R. King. Extensions of adaptive slope-seeking for active flow control. *Accepted for Journal of Systems and Control Engineering*, 2008.

[22]L. Henning and R. King. Drag reduction by closed-loop control of a separated flow over a bluff body with a blunt trailing edge. In *44th IEEE Conference on Decision and Control and European Control Confernce ECC 2005*, Seville, Spain, 2005.

[23]L. Henning and R. King. Robust multivariable closed-loop control of a turbulent backward-facing step flow. *AIAA Journal of Aircraft*, 40:201–208, 2007.

[24]R. King. *Active Flow Control*. Springer-Verlag, Berlin, 2007.

[25]R. King, R. Becker, G. Feuerbach, L. Henning, R. Petz, W. Nitsche, O. Lemke, and W. Neise. Adaptive flow control using slope seeking. In *14th IEEE Mediterranean Conference on Control Automation*, Ancona, 2006.

[26]R. King, M. Seibold, O. Lehmann, B. R. Noack, M. Morzyński, and G. Tadmor. Nonlinear flow control based on a low dimensional model of fluid flow. In T. Meurer, K. Graichen, and E. D. Gilles, editors, *Control and Observer Design for Nonlinear Finite- and Infinite-Dimensional Systems*, pages 369–386. Springer, 2005.

[27]M. Kloker. A robust high-resolution split-type compact FD-scheme for spatial direct numerical simulation of boundary-layer transition. *Appl. Sci. Research*, 59(4):353–377, 1998.

[28]T. C. Lieuwen and V. Yang, editors. *Combustion Instabilities in Gas Turbine Engines*, volume 210 of *Progress in Astronautics and Aeronautics*. AIAA, Inc., 2005.

[29]J. P. Moeck, M. R. Bothien, C. O. Paschereit, G. Gelbert, and R. King. Two-parameter extremum seeking for control of thermoacoustic instabilities and characterization of linear growth. 2007. AIAA Paper 2007-1416.

[30]A. S. Morgans and A. P. Dowling. Model-based control of combustion instabilities.

[31]M. Morzyński, K. Afanasiev, and F. Thiele. Solution of the eigenvalue problems resulting from global non-parallel flow stability analysis. *Comput. Meth. Appl. Mech. Enrgrg.*, 169:161–176, 1999.

[32]R. Muminovic, L. Henning, R. King, A. Brunn, and W. Nitsche. Robust and model predictive drag control for a generic car model. In *AIAA 4th Flow Control Conference 2008-3859*, 2008.

[33]B. R. Noack, M. Schlegel, B. Ahlborn, G. Mutschke, M. Morzyński, P. Comte, and G. Tadmor. A finite-time thermodynamics of unsteady fluid flows. *J. Non-Equilibr. Thermodyn.*, To appear in Volume 33(2), 2008.

[34]B.R. Noack, K. Afanasiev, M. Morzyński, G. Tadmor, and F. Thiele. A hierarchy of low-dimensional models for the transient and post-transient cylinder wake. *J. Fluid. Mech.*, 497:335–363, 2003.

[35]M. Pastoor, L. Henning, B.R. Noack, R. King, and G. Tadmor. Feedback shear layer control for bluff body drag reduction. *J. Fluid. Mech.*, accepted.

[36]T. J. Poinsot, A. C. Trouve, D. P. Veynante, S. M. Candel, and E. J. Esposito. Vortex-driven acoustically coupled combustion instabilities.

[37] S. Qin and T. Badgewell. An overview of industrial model predictive control technology. In *AIChE Symposium Series - American Institute of Chemical Engineers*, pages 232–256. AIChE, 1997.

[38] J. B. Rawlings. Tutorial overview of model predictive control. *IEEE Control Systems Magazine*, 20(3):38–52, 2000.

[39] U. Rist and H. Fasel. Direct numerical simulation of controlled transition in a flat-plate boundary layer. *J. Fluid Mech.*, 298:211–248, 1995.

[40] M. Samimy, M. Debiasi, Caraballo, A. E.ãndSerrani, X. Yuan, J. Little, and J. Myatt. Feedback control of subsonic cavity flows using reduced-order models. *J. Fluid Mech.*, 579:315–346, 2007.

[41] S. Siegel, K. Cohen, and T. McLaughlin. Feedback control of a circular cylinder wake in experiment and simulation. *AIAA-Paper 2003-3569*, 2003.

[42] D. Sturzebecher and W. Nitsche. Active cancellation of tollmien-schlichting instabilities on a wing using multi-channel sensor actuator system. *Int. J. Heat and Fluid Flow*, 24(4):572–583, 2003.

[43] W. Waldraff, R. King, and E.D. Gilles. Optimal feeding strategies by adaptive mesh selection for fed-batch bioprocesses. *Bioprocess Engineering*, 17(4):221–227, 1997.

[44] H.-H. Wang, S. Yeung, and M. Krstic. Experimental application of extremum seeking on an axial flow compressor. In *Proc. of the American Control Conference 1998*, Philadelphia, Pennsylvania, U.S.A., 1998.

[45] K.E. Wu and K.S. Breuer. Control of boundary layer using FXLMS feedforward architectures. *AIAA-Paper 2006-3022*, 2006.